# VALIDATION OF A TIME-DEPENDENT MODEL FOR THERMOPLASTIC-BASED LAMINATES AT TEMPERATURES HIGHER THAN Tg: HIGH STRESS GRADIENT STRUCTURES AND DIGITAL IMAGE CORRELATION

B. Vieille*, W. Albouy, L. Taleb

*Groupe de Physique des Matériaux UMR 6634 CNRS, INSA Rouen Avenue de l'Université 76801 Saint Etienne du Rouvray, France*
**benoit.vieille@insa-rouen.fr*

**Keywords:** thermoplastic, viscous behavior, finite element analysis, high gradient structures

**Abstract**
This study was aimed at validating a time-dependent model accounting for the influence of viscous effects of PPS matrix on the behaviour of C/PPS laminates at temperatures exceeding its $T_g$, when matrix viscoelasticity and viscoplasticity are prominent. This numerical model combines a linear spectral viscoelastic model and a generalized Norton-type viscoplastic model, and was implemented into the Finite Element code Cast3m. A Digital Image Correlation technique was used to validate the model's ability to predict the response of TP-based laminates subjected to complex stress states at $T>T_g$.

## 1. Introduction

High-performance thermoplastic (TP) resins, such as polyetheretherketone (PEEK) and polyphenylenesulfide (PPS), offer a promising alternative to thermosetting (TS) resins such as epoxies: high degree of chemical resistance, excellent damage and impact resistance, and they may be used over a wide range of temperatures [1]. In addition, it is well established that physical properties (Crystallinity rate and glass transition temperature $T_g$) of TP resins are closely associated with the mechanical behavior of Polymer Matrix Composites (PMCs) under high temperatures [2]. An overview of environment effects on performance of PMCs (TS and TP) is presented in [3]. Around their $T_g$, the nonlinear behavior (plastic and time-dependent behaviors) of fiber-reinforced polymer composites becomes significant, especially under off-axis loading conditions. This nonlinear response, associated with the shear deformation of the polymer matrix along reinforcing fibers, is enhanced at high temperature depending on matrix nature and loading conditions [4-13]. While the ability to predict the behavior of composite structures is a major issue in design of engineering structures, there is still a lack of confidence into existing approaches for stress field analysis, especially for high gradient structures. Thus, there is a need to develop reliable numerical tools to account for their visco-elastic-plastic behaviours when materials are subjected to stress heterogeneities [14,15,16]. Over the past decades, several authors attempted to describe the time-dependent

behaviour of PMCs. For relatively low loading levels, the viscous behaviour is described as linear or nonlinear viscoelastic [17]. From the simple rheological formulation to the more complex approach of Schapery's model [18], most of the viscoelastic models comes from polymers and was later adapted and extended to composite materials. When the load increases, viscoelastic models lose their accuracy, as the viscoplastic behaviour becomes predominant. Finally, most of the viscoelastic viscoplastic models are not able to predict accurately the viscous behaviours at the vicinity of $T_g$ [19].

## 2. Experimental investigations

### *2.1. Materials and specimens*

The composite material studied in this work consists of a carbon fabric reinforced PPS prepreg laminates, whose fibers volume fraction is 50%. The reinforcement is a 5-harness satin weave of T300 3K carbon fibers supplied by Soficar and the matrix is a high performance TP (PPS) supplied by Ticona company, referenced as Fortron 0214. The material's glass transition temperature is 95°C [14]. Tests were performed on $[(+45,-45)]_7$ specimens, whose viscous behaviour is exacerbated at temperatures higher than $T_g$.

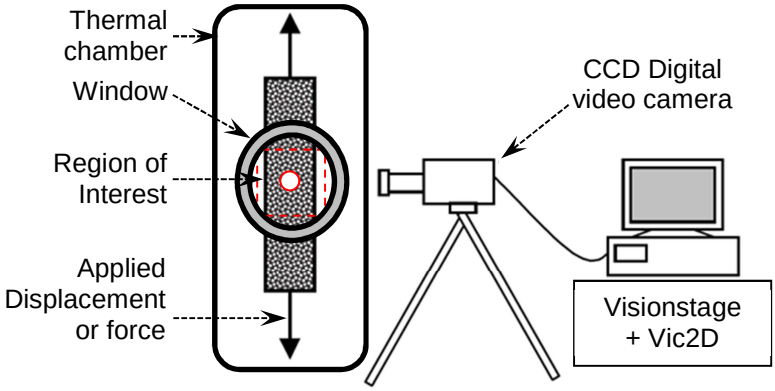


**Figure 1.** Digital Image Correlation techniques for strain field measurements: experimental set-up

### *2.2. Experimental procedure*

All the tests were performed using a 100 kN capacity load cell of a MTS 810 servo-hydraulic testing machine with a temperature control system. Tensile loadings were applied to high gradient structures: perforated [15,16] and double-notched [20]. Monotonic, creep-recovery and multi-relaxation tests have been performed at 120°C (service temperature for aircraft engine nacelles). Among the different methods available to localize or identify the damage induced by mechanical loading in high gradient structures, a Digital Image Correlation (DIC) technique can be considered because of its simplicity, its good accuracy and its ability to measure full-field strains [21,22], even at high temperatures [15,16,23]. During tensile loading, a Region Of Interest (ROI) is filmed near the geometrical singularity (see Fig. 1) with a CCD video camera (659*493 pixels resolution), and through the window of the thermal chamber.

## 3. Numerical modelling

### *3.1 Constitutive laws of a time-dependent model*

In order to apprehend the viscous behaviours of C/PPS laminates at $T>T_g$, a numerical modelling consisting of a viscoelastic spectral and a generalized Norton-type viscoplastic formulation developed for TS-based composites have been adopted [14]. Under the assumption of small strains, the total strain is usually divided into three different parts:

$$\underline{\varepsilon} = \underline{\varepsilon}^{e} + \underline{\varepsilon}^{ve} + \underline{\varepsilon}^{vp} \quad (1)$$

#### *3.1.1 Viscoelastic model*

In order to predict the viscoelastic behavior of PMCs, a viscoelastic spectral linear model was used [14]. It lays on a decomposition of the viscoelastic strain rate $\underline{\dot{\varepsilon}}^{ve}$ in elementary mechanisms $\underline{\xi}_i$ associated with a relaxation time spectrum:

$$\underline{\dot{\varepsilon}}^{ve} = \sum_{i=1}^{n_b} \underline{\dot{\xi}}_i \quad (2)$$

The viscoelastic formulation assumes a Gaussian distribution (see Fig. 2) of the relaxation mechanisms weights according to $\tau_i = \exp(n(i))$, relaxation time of the i$^{th}$ mechanism.

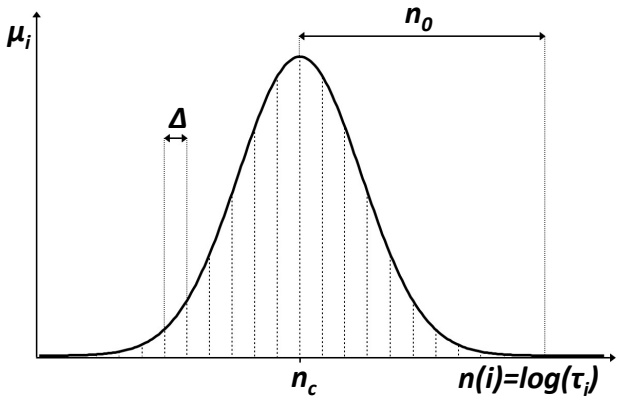


**Figure 2.** Gaussian spectral lay-out of the viscous relaxation mechanisms

The distribution is characterized by two parameters: $n_0$ (standard deviation) and $n_c$ (average). From a physical point of view, the value of $n_0$ gives an enhanced effect on late mechanisms, whereas an increase in the value of $n_c$ tends to homogenize the weights of the viscous mechanisms (see Fig. 2). $\Delta$ being the interval between two relaxation times, $\tau_i$ can be obtained from the definition of $n(i)$ such as:

$$\mathrm{n(i)} = n_c - n_0 + (i-1)\Delta \quad \text{with} \quad \Delta = \frac{2n_0}{n_b - 1} \quad (3)$$

From this definition, the weights $\mu_i$ of viscous mechanisms can be calculated from:

$$\mu_i = \frac{1}{n_0\sqrt{\pi}} \times \exp\left(-\left(\frac{n(i)-n_c}{n_0}\right)^2\right) \quad (4)$$

Once each mechanism is identified on the spectrum, it must comply with the following differential equation deriving from a thermodynamic potential:

$$\dot{\underline{\xi}}_i = \frac{1}{\tau_i}\left(\mu_i \underline{\underline{S}}^{ve}\underline{\sigma} - \underline{\xi}_i\right) \tag{5}$$

where $\underline{\sigma}$ is the Cauchy stress tensor and $\underline{\underline{S}}^{ve}$ is the viscoelastic compliances tensor associated with a viscous anisotropy tensor $\underline{\underline{A}}^{ve}$ such as $\underline{\underline{S}}^{ve} = \underline{\underline{A}}^{ve-1}$:

$$\underline{\underline{S}}^{ve} = \begin{bmatrix} 0 & 0 & 0 & 0 & 0 & 0 \\ 0 & \beta_{22}/E_2 & (-\beta_{23}.\nu_{23})/E_2 & 0 & 0 & 0 \\ 0 & (-\beta_{23}.\nu_{23})/E_2 & \beta_{22}/E_3 & 0 & 0 & 0 \\ 0 & 0 & 0 & \beta_{44}/G_{12} & 0 & 0 \\ 0 & 0 & 0 & 0 & \beta_{44}/G_{12} & 0 \\ 0 & 0 & 0 & 0 & 0 & \beta_{66}/G_{23} \end{bmatrix}$$

where $\beta_{22}$, $\beta_{23}$, $\beta_{44}$, $\beta_{66} = 2\beta_{22}G_{23}/E_2$ are parameters representing material's viscosity, and ($E_2$, $G_{12}$, $G_{23}$) are stiffness modulus.

*3.1.2 Viscoplastic model*

The viscoelastic spectral model is completed with a generalized Norton-type viscoplastic model [14]:

$$f_{vp}(\underline{\sigma}, \underline{X}) = \overline{(\underline{\sigma} - \underline{X})} - \tau_y(T) \text{ with } \overline{(\underline{\sigma} - \underline{X})} = \sqrt{{}^T(\underline{\sigma} - \underline{X})\underline{\underline{M}}(\underline{\sigma} - \underline{X})} \tag{6}$$

Where $\underline{\underline{M}}$ is a fourth order tensor describing the anisotropy of viscoplastic flow in shear loading associated with the PPS matrix. In the case of a linear kinematics hardening, the thermodynamic force $\underline{X}$ associated with $\underline{\alpha}$ is defined by $\underline{X} = \delta\underline{\alpha}$. The evolution laws derived from a thermodynamic potential can be written for $\underline{\dot{\varepsilon}}^{vp}$ the viscoplastic strain rate and $\underline{\dot{\alpha}}$ the kinematic hardening rate:

$$\underline{\dot{\varepsilon}}^{vp} = \dot{\lambda}_{vp}\frac{\underline{\underline{M}}(\underline{\sigma}-\underline{X})}{\overline{(\underline{\sigma}-\underline{X})}} \quad \text{and} \quad \underline{\dot{\alpha}} = \dot{\lambda}_{vp}\frac{\underline{\underline{M}}(\underline{\sigma}-\underline{X})}{\overline{(\underline{\sigma}-\underline{X})}} = \underline{\dot{\varepsilon}}^{vp} \tag{7}$$

where $\dot{\lambda}_{vp} = \sqrt{{}^T\underline{\dot{\varepsilon}}^{vp}\underline{\underline{M}}^{-1}\underline{\dot{\varepsilon}}^{vp}}$ is the Lagrange viscoplastic multiplier homogenous to a strain rate. The viscoelastic and viscoplastic model parameters can be identified from a purely viscoelastic creep tests, and monotonic tensile tests at different strain rates respectively. The parameter **δ** can be identified from a gradual load-unload tensile test.

| $E_1$ (GPa) | $E_2$ (GPa) | $G_{12}(T)$ (GPa) | $\nu_{12}$ | $\tau_y(T)$ (MPa) | $n_0$ | $n_c$ | $\beta_{44}$ | δ (MPa) | $K$ | $N$ |
|---|---|---|---|---|---|---|---|---|---|---|
| 56.5 | 56.5 | 1,35 | 0.04 | 10 | 4.05 | 6.9 | 0.6 | 400 | $8.4e^{-12}$ | 9,5 |

**Table 1.** Mechanical properties of the elementary ply and identified model parameters [14]

### *3.1.3 Time Discretization*

The previous constitutive laws have been time-discretized (backward Euler) and implemented into a FE code (Cast3m). For an incremental method associated with a Newton iterative scheme, the material state has to be calculated on a time interval $[t_n, t_{n+1}]$ from a strain increment $\Delta\underline{\varepsilon}$, knowing the previous converging state :

$$\left({}_n\underline{\sigma},\ {}_n\underline{\xi}_i,\ {}_n\underline{X}\right) + \Delta\underline{\varepsilon} \rightarrow \left({}_{n+1}\underline{\sigma},\ {}_{n+1}\underline{\xi}_i,\ {}_{n+1}\underline{X}\right) \tag{8}$$

with ${}_n(.)$ and ${}_{n+1}(.)$ representing respectively the previous convergent quantities and the current ones. At the end of each increment, the state of the material is calculated from a classical return-map algorithm. It consists in assuming an elastic state, which can be followed by a correction phase to comply with the yield function if the latter is violated. The viscoplastic multiplier ${}_{n+1}\dot{\lambda}_{vp}$ is calculated by enforcing the condition $f_{vp}^{d}\left({}_{n+1}\underline{\sigma},\ {}_{n+1}\underline{X},\ {}_{n+1}\dot{\lambda}_{vp}\right) = 0$ at the end of the time step.

### *3.2 Validation of the numerical modelling*

#### *3.2.1 Monotonic tensile tests on double-notched laminates*

In order to validate this model, tensile tests have been carried out on double-notched laminates at 120°C. The experimental and numerical stress-strain responses have been compared (see Fig. 3a). The purpose is to evaluate the notch sensitivity (defined by $C_h = \sigma^{notched}/\sigma^{unnotched}$) of C/PPS laminates. $C_h$ depends on the ability of the material to accommodate overstresses near the notch, and is associated with matrix ductility and toughness [16].

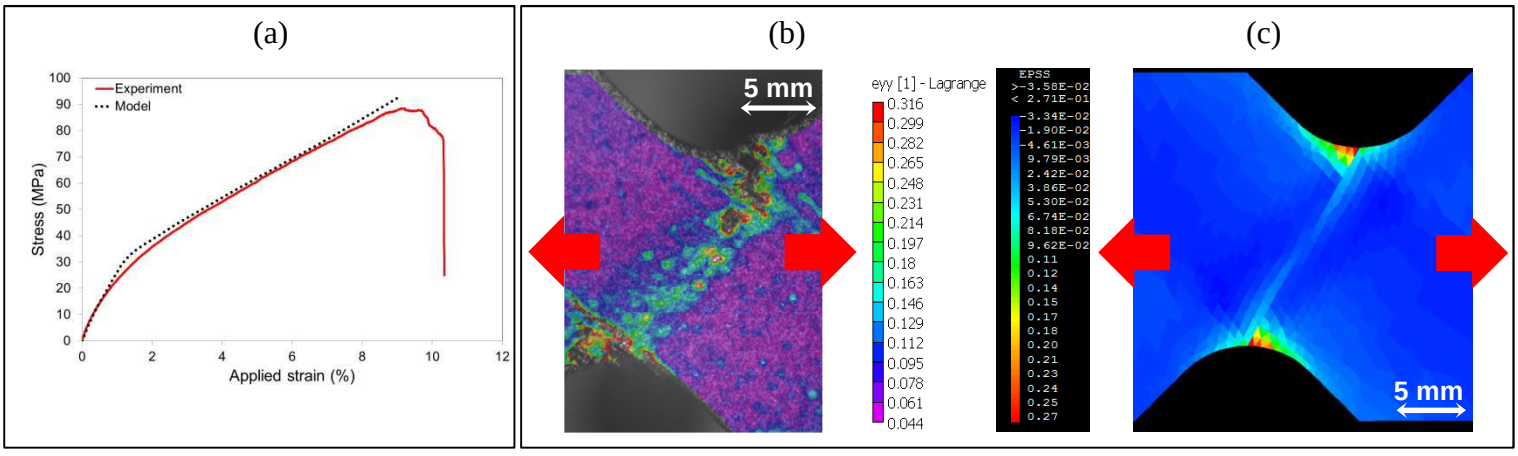


**Figure 3.** (a) Macroscopic response of double-notched laminates subjected to a monotonic tensile loading – Comparison of the longitudinal Green-Lagrange strain fields $E_{yy}$ at failure on double-notched laminates subjected to a monotonic tensile loading: (b) DIC from experimental data – (c) numerical modelling

From the longitudinal Green-Lagrange strain fields (see Fig. 3b and 3c), it appears that high gradient structures experience specific viscous mechanisms along the ±45° oriented fibers,

which are instrumental in accommodating overstresses near the hole, ultimately resulting in lower notch sensitivity. The comparison of DIC results and numerical modelling shows that the longitudinal Green-Lagrange strain fields $E_{yy}$ at failure are in good agreement from qualitative and quantitative standpoints. These results show that the numerical model adequately predicts the response of TP-based laminates subjected to complex stress states at the vicinity of $T_g$.

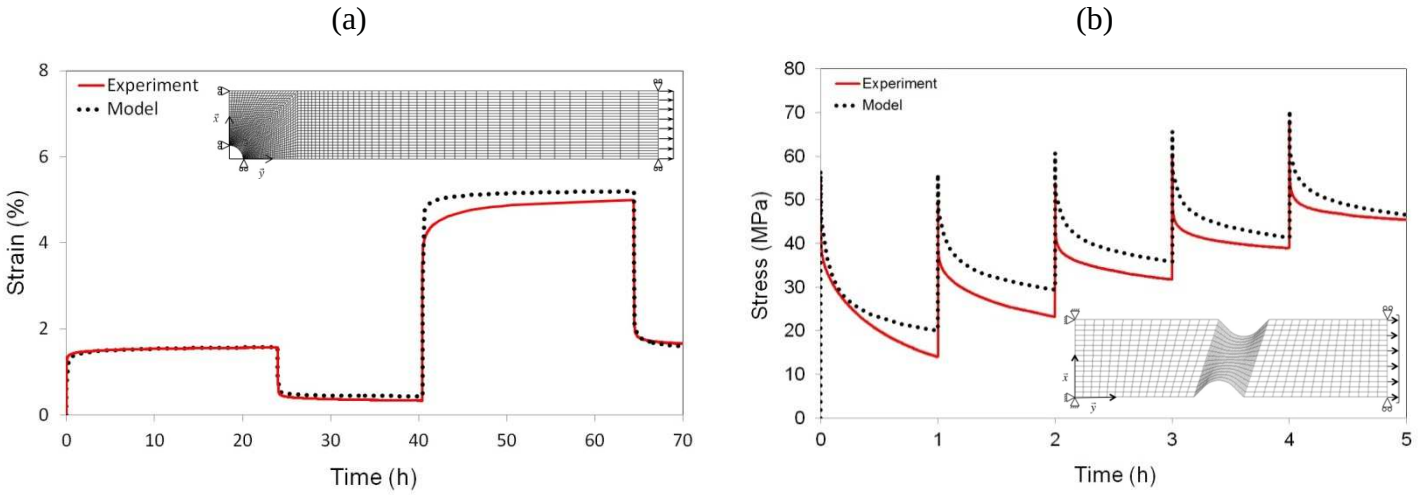


**Figure 4.** Response of notched C/PPS laminates at 120°C: (a) creep-recovery test – (b) multi-relaxation test

### *3.2 Long-term behaviour of notched laminates*

The response of perforated C/PPS laminates subjected to a creep-recovery loading, has been simulated (see Fig. 4a). Two successive creep-recovery tests were performed at 120°C and for stress levels equal to 40 and 80 MPa respectively, during 24 hours [14]. One quarter of the specimen was meshed with 960 four-node shell elements.

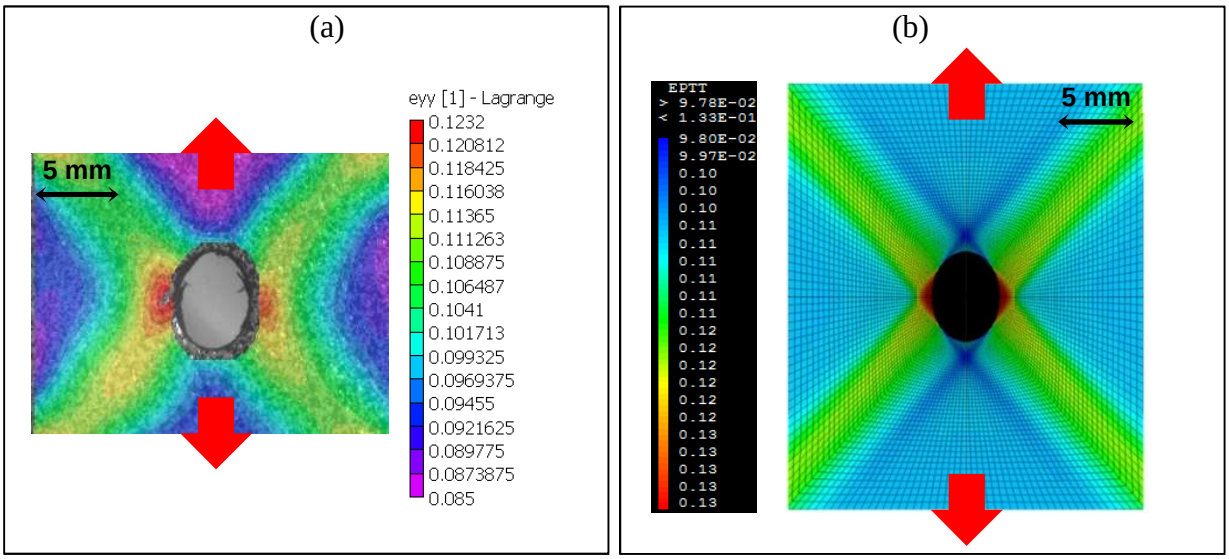


**Figure 5.** Comparison of the longitudinal Green-Lagrange strain fields $E_{yy}$ after 24h during a creep-recovery tests on notched laminates at 120°C: (a) DIC from experimental data – (b) numerical modelling

In addition, a double-notched laminates has been subjected to a multi-relaxation loading at strain levels equal to 2-3-4-5-6% respectively (see Fig. 4b). The specimen was meshed with 1350 four-node shell elements. Once again, the comparison of numerical and experimental results shows that the longitudinal strain fields after a 24h creep loading are in good agreement (see Fig. 5). The numerical model confirms that cumulative visco-elastic-plastic deformations develop along the ±45° oriented fibers bundles, due to the highly ductile behavior of PPS matrix enhanced at 120°C. From the obtained results, it appears that the model adequately simulates the time-dependent behaviour of high gradient structures at $T>T_g$.

## 4. Conclusion

The present work was aimed at validating the applicability of a time-dependent model in the case of TP-based composites at $T> T_g$, when most models proposed in the literature lose their predictive capacity. A numerical modelling consisting of a viscoelastic spectral and a generalized Norton-type viscoplastic formulation has been adopted. The responses of notched C/PPS laminates subjected to various loadings (monotonic tensile, creep-recovery and multi-relaxation test) have been simulated. A Digital Image Correlation technique has been used to validate the model's ability to predict the time-dependent response of high gradient structures subjected to tensile loadings. For the different tests, the comparison of DIC results and numerical modelling shows that the longitudinal Green-Lagrange strain fields $E_{yy}$ are in good agreement from qualitative and quantitative standpoints. Finally, the proposed modelling proved to be promising to adequately predict the behavior of TP-based laminated at $T> T_g$, even in the case of structural testing.

## References

[1] R. Vodicka. Thermoplastics for Airframe Applications. A review of the properties and repair methods for thermoplastic composites. *Technical Report* n° DSTO-TR-0424, Australian Government of Defense, 2006.

[2] J.E. Spruiell, C.J. Janke. A review of the measurement and development of crystallinity and its relation to properties in neat PPS and its fiber reinforced composites. *Technical Report*, Metals and Ceramics Division, US Dept of Energy, 2004.

[3] N.L. Hancox. Overview of effects of temperature and environment on performance of polymer matrix composite properties. *Plastics Rubber and Composites Process and Applications*, 27(3):97-106, 1998.

[4] M. Kawai, S. Yajima, A. Hachinohe, Y. Kawase. High-temperature off axis fatigue behaviour of unidirectional CFR composites with different resin matrices. *Composites Sciences and Technology*, 61: 1285-1302, 2001.

[5] M.C. Lafarie-Frenot, F. Touchard. Comparative in-plane shear behaviour of long-carbon-fibre composites with TS or TP matrix. *Composites Sciences and Technology*, 52(3):417-425, 1994.

[6] S. Deng, X. Li, H. Lin, J. Weitsman. The non-linear response of quasi-isotropic composite laminates. *Composites Sciences and Technology*, 64(10-11): 1577-1585, 2004.

[7] S.K. Ha, Q. Wang, F.K. Chang. Modeling the viscoplastic behavior of fiber-reinforced TP matrix composites at elevated temperatures. *Journal of Composite Materials*, 25(4):334-374, 1991.

[8] M.H.R. Jen, Y.C. Tseng, S.C. Chang, M. Chen. Mechanical properties in notched AS4/PEEK APC2 composite laminates at elevated temperature. *Journal of Composite Materials*, 40(11): 955-969, 2006.

[9] I. De Baere, W. Van Paepegem, J. Degrieck. Modeling the nonlinear shear stress-strain behavior of a CFR PPS from rail shear and $[45,-45]_{4S}$ tensile test. *Polymer Composites*, 1016-1026, 2009.

[10] D. Meyer, H. Bersee, A. Beukers. Temperature effect on reinforced TP composite properties for primary aircraft structure applications. In: Proceedings of 49th Structural Dyn. and Mat. Conference, Seattle, WA, April, 2008.

[11] J.S. Loverich, B.E. Russel, S.W. Case, K.L. Reifnider. Life of PPS composites subjected to cyclic loading at elevated temperatures. Time dependent and nonlinear effects. *Polymer Composites*:310-317, 2000.

[12] C.A. Mahieux, C. Scheurer. Elevated temperature bending stress rupture behavior AS4/APC2 and comparison with AS4/PPS. *Composites Part A*, 33:935-938, 2002.

[13] S.J. Kim, J.Y. Cho. Role of matrix in viscoplastic behavior of thermoplastic composites at elevated temperature. *AIAA Journal*, 30(10), 1992.

[14] W. Albouy, B. Vieille, L. Taleb. Experimental and numerical investigations on the time-dependent behavior of woven-ply PPS thermoplastic laminates at temperatures higher than glass transition temperature. *Composites Part A*, 49:165-178, 2013.

[15] B. Vieille, L. Taleb. About the influence of temperature and matrix ductility on the behavior of carbon woven-ply PPS or epoxy laminates: Notched and unnotched laminates. *Composites Science and Technology*, 71(7):998-1007, 2011.

[16] B. Vieille, J. Aucher, L. Taleb. Overstress accommodation in notched woven-ply thermoplastic laminates at high-temperature: Numerical modeling and validation by Digital Image Correlation. *Composites Part B*, 45(1):290-302, 2013.

[17] W.N. Findley, J.S. Lai, K. Onaran. Creep and relaxation of nonlinear viscoelastic materials : with an introduction to linear viscoelasticity. North-Holland Pub. Co., 1976.

[18] R.A. Schapery. Nonlinear viscoelastic and viscoplastic constitutive equations based on thermodynamics. *Mechanics of Time-Depend Materials*, 1(2):209-40, 1997.

[19] M.S. Al-Haik, M.Y. Hussaini, H. Garmestani. Prediction of nonlinear viscoelastic behavior of polymeric composites using an artificial neural network. *International Journal of Plasticity*, 22(7):1367-92, 2006.

[20] M.H.H. Meuwissen, C.W.J. Oomens, F.P.T. Baaijens, R. Petterson, J.D. Janssen. Determination of the elasto-plastic properties of aluminium using a mixed numerical-experimental method. *Journal of Materials Processing Technology*, 75(1):204-211, 1998.

[21] F. Meraghni, H. Nouri, N. Bourgeois, C. Czarnota, P. Lory. Parameters identification of fatigue damage model for short glass fiber reinforced polyamide (PA6-GF30) using digital image correlation. *Procedia Engineering*, 10:2110-2116, 2011.

[22] F. Lagattu F, M.C. Lafarie-Frenot, T.Q. Lam, J. Brillaud. Experimental characterisation of overstress accommodation in notched CFRP composite laminates. *Composite Structures*, 67:347-357, 2005.

[23] J.S. Lyons, J. Liu, M.A. Sutton. High-temperature deformation measurements using digital-image correlation. *Experimental Mechanics*, 36(1):64-70, 1996.